nature materials

Letter

https://doi.org/10.1038/s41563-023-01502-7

Single-crystalline van der Waals layered dielectric with high dielectric constant

Received: 9 July 2022

Accepted: 9 February 2023

Published online: 9 March 2023

Check for updates

Congcong Zhang[1,11], Teng Tu[1,11], Jingyue Wang[1,11], Yongchao Zhu[1,2,11], Congwei Tan[1], Liang Chen[3], Mei Wu[4], Ruixue Zhu[4], Yizhou Liu[5], Huixia Fu[5,6], Jia Yu[7], Yichi Zhang[1], Xuzhong Cong[1], Xuehan Zhou[1], Jiaji Zhao[8], Tianran Li[1], Zhimin Liao[8], Xiaosong Wu[8], Keji Lai[7], Binghai Yan[5], Peng Gao[4], Qianqian Huang[3], Hai Xu[2], Huiping Hu[2], Hongtao Liu[1], Jianbo Yin[9,10,11] & Hailin Peng[1,10] ✉

The scaling of silicon-based transistors at sub-ten-nanometre technology nodes faces challenges such as interface imperfection and gate current leakage for an ultrathin silicon channel[1,2]. For next-generation nanoelectronics, high-mobility two-dimensional (2D) layered semiconductors with an atomic thickness and dangling-bond-free surfaces are expected as channel materials to achieve smaller channel sizes, less interfacial scattering and more efficient gate-field penetration[1,2]. However, further progress towards 2D electronics is hindered by factors such as the lack of a high dielectric constant (κ) dielectric with an atomically flat and dangling-bond-free surface[3,4]. Here, we report a facile synthesis of a single-crystalline high-κ (κ of roughly 16.5) van der Waals layered dielectric Bi_2SeO_5. The centimetre-scale single crystal of Bi_2SeO_5 can be efficiently exfoliated to an atomically flat nanosheet as large as 250 × 200 μm^2 and as thin as monolayer. With these Bi_2SeO_5 nanosheets as dielectric and encapsulation layers, 2D materials such as Bi_2O_2Se, MoS_2 and graphene show improved electronic performances. For example, in 2D Bi_2O_2Se, the quantum Hall effect is observed and the carrier mobility reaches 470,000 $cm^2 V^{-1} s^{-1}$ at 1.8 K. Our finding expands the realm of dielectric and opens up a new possibility for lowering the gate voltage and power consumption in 2D electronics and integrated circuits.

The search for high-dielectric-constant (κ) dielectric materials and adapting them to channel materials have been core tasks since the birth of the transistor[1,3,5]. This becomes vital when device scale is being thinned to an atomic level such as in two-dimensional (2D) electronics because the charge carriers will be more sensitive to scattering centres at dielectric channel interfaces: for instance, strain, dangling bonds and impurities[4,6]. Therefore, van der Waals (vdW) dielectrics with dangling-bond-free and atomically flat surfaces are more suitable for

[1]Center for Nanochemistry, Beijing Science and Engineering Center for Nanocarbons, Beijing National Laboratory for Molecular Sciences, College of Chemistry and Molecular Engineering, Peking University, Beijing, China. [2]College of Chemistry and Chemical Engineering, Central South University, Changsha, China. [3]School of Integrated Circuits, Peking University, Beijing, China. [4]Electron Microscopy Laboratory, School of Physics and International Center for Quantum Materials, Peking University, Beijing, China. [5]Department of Condensed Matter Physics, Weizmann Institute of Science, Rehovot, Israel. [6]College of Physics and Center for Quantum Materials and Devices, Chongqing University, Chongqing, China. [7]Department of Physics, University of Texas at Austin, Austin, TX, USA. [8]State Key Laboratory for Mesoscopic Physics and Frontiers Science Center for Nano-optoelectronics, School of Physics, Peking University, Beijing, China. [9]School of Electronics, Peking University, Beijing, China. [10]Beijing Graphene Institute, Beijing, China. [11]These authors contributed equally: Congcong Zhang, Teng Tu, Jingyue Wang, Yongchao Zhu, Jianbo Yin. ✉e-mail: hlpeng@pku.edu.cn

https://doi.org/10.1038/s41563-023-01502-7

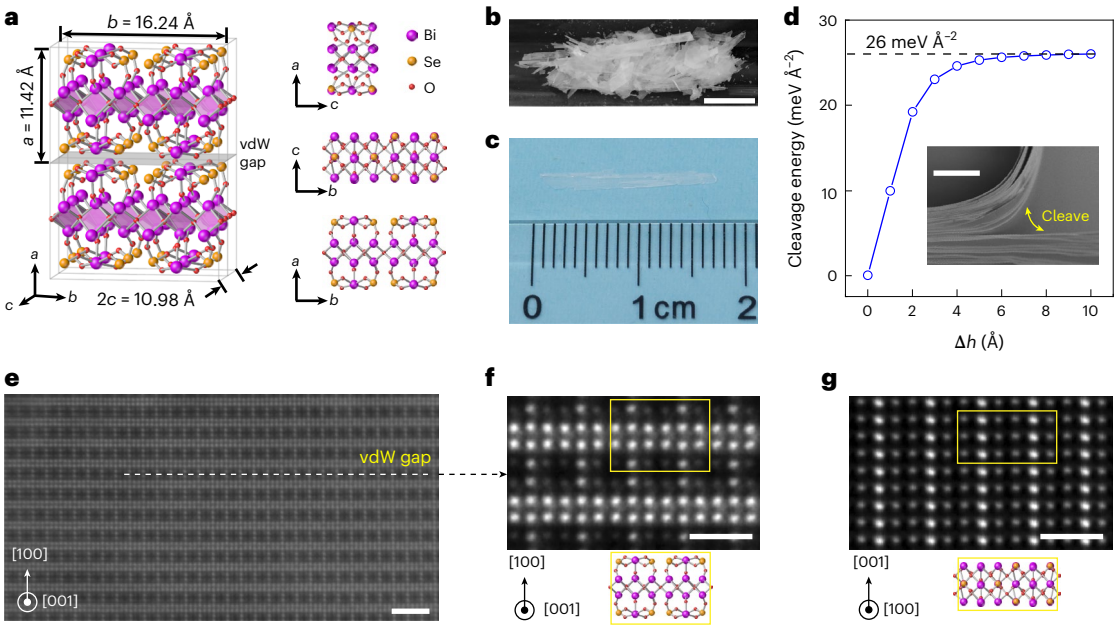

Fig. 1 | Structure and characterization of vdW layered Bi_2SeO_5 single crystals. **a**, Crystal structure of Bi_2SeO_5. The vdW gap is marked with a grey plane in the left panel. **b**, Photograph of as-grown crystals. Scale bar, 1 cm. **c**, A typical crystal with length reaching 1.7 cm. **c**, A typical crystal reaches 1.7 cm in length. **d**, Cleavage energy of Bi_2SeO_5 crystal, 26 meV $Å^{-2}$. The inset shows an scanning electron microscopy image of a half-cleaved crystal. Scale bar, 20 μm. **e**, Cross-sectional HAADF–STEM image of a Bi_2SeO_5 nanosheet, showing a layered structure. The vdW gap is marked by a white dotted line. Scale bar, 2 nm. **f**, High-magnification image of **e**. **g**, HAADF–STEM image of (100) plane. The unit cell along the [001] direction (**f**) and [100] direction (**g**) is marked with a yellow box. Scale bars in **f** and **g**, 1 nm.

2D electronics than those used in the Si industry (HfO_2, SiO_2 and so on). For example, hexagonal boron nitride (hBN)[7–11] has been widely used as a vdW dielectric in devices to achieve high carrier mobility (even phonon-limited mobility)[12,13], enabling research on quantum Hall effects (QHEs)[14,15], 2D superconductivity[16], 2D ferromagnetism[17] and moiré physics[18]. Given that the hBN has relatively low dielectric constant (κ roughly 3.5), great effort has been devoted to finding new high-κ vdW layered dielectrics with dangling-bond-free atomically smooth surfaces and high breakdown field strengths (E_{bd}) so that stronger gate control and thus lower operating voltage can be achieved. Recent progress includes the discovery of layered transitional metal oxides such as MoO_3, V_2O_5 and WO_3 (refs. [4,19]), which show great potential but bear possible current leakage arising from neutral oxygen vacancies in this group of oxides[20,21].

Here, we report the synthesis of centimetre-scale single crystals of layered high-κ insulator bismuth selenite (Bi_2SeO_5) via a facile chemical vapour transport (CVT) method. The as-synthesized single crystal of Bi_2SeO_5 has a typical size on centimetre scale. Owing to its vdW layered structure and small cleavage energy (26 meV $Å^{-2}$), the bulk crystal can be efficiently exfoliated to an atomically flat nanosheet as large as 250 × 200 $μm^2$ and as thin as monolayer. The out-of-plane dielectric constant and breakdown field strength are measured as about 16.5 and above 10 MV cm^{-1}, respectively. We further show that a Bi_2SeO_5 nanosheet can serve as the encapsulation layer and gate dielectric for 2D semiconductors. Its high κ value allows strong gate control of charge carriers and reduced scattering in the encapsulated device. Meanwhile, an atomically flat surface of the dielectric enhances the mobility by 250% and guarantees the observation of pronounced Shubnikov–de Haas (SdH) oscillations and QHE in 2D Bi_2O_2Se devices, the latter of which has never been observed in 2D Bi_2O_2Se before.

Bi_2SeO_5 crystallizes in the orthorhombic lattice with an *Abm*2 space group (a = 11.42 Å, b = 16.24 Å, c = 5.49 Å, Z = 8)[22,23], and adopts a vdW layered structure with a covalently saturated surface in the [100] direction, as shown in Fig. 1a and Supplementary Table 2. Flake-shaped crystals of Bi_2SeO_5 were grown by the facile CVT method at roughly 860 °C in which iodine (I_2) and Bi_2SeO_5 polycrystalline powder served as a transport agent and source, respectively (Methods). The crystal phase and lattice parameters of the grown Bi_2SeO_5 flakes ($a \cong 11.44$ Å, $b \cong 16.28$ Å, $c \cong 5.49$ Å, $Z = 8$) were determined by single-crystal X-ray diffraction (XRD) analysis. These single-crystalline Bi_2SeO_5 flakes have dimensions of up to 0.2 × 1.7 cm^2 as shown in Fig. 1b,c, which are much larger than hBN bulk single crystals widely used in 2D electronics. The Bi_2SeO_5 flakes were further confirmed to be layered single crystals by the intense and sharp peaks that are exclusively assigned to (h00) crystal planes in XRD analysis (Supplementary Fig. 1). As the vdW gap is parallel to the (100) crystal plane and the calculated cleavage energy of 26 meV $Å^{-2}$ is comparable to hBN, Bi_2SeO_5 flakes can be easily cleaved into thin layers (Fig. 1d).

The single-crystalline nature and existence of the vdW gap in layered Bi_2SeO_5 are further confirmed by transmission electron microscopy of exfoliated Bi_2SeO_5 nanosheets. The cross-sectional high-angle annular dark field–scanning transmission electron microscopy (HAADF–STEM) images show (001) planes with a vdW gap (Fig. 1e,f) and (100) planes (Fig. 1g) that correspond to the side and top views of the crystal flake, respectively. The HAADF–STEM images in Supplementary Fig. 1 reveal lattice constants of $a \cong 11.2$ Å and $b \cong 15.9$ Å, consistent with XRD results (Supplementary Information, Discussion S1).

The small cleavage energy (Fig. 1d and Supplementary Fig. 3) of single-crystalline Bi_2SeO_5 vdW layers enables a facile mechanical exfoliation of large-area ultraflat nanosheets from Bi_2SeO_5 bulk to target substrate. The first contact of an adhesive tape on the crystal has already peeled off millimetre-sized films as shown in Fig. 2a,b. Repeatedly folding the tapes and then pressing them on Si/SiO_2 leaves nanosheets with typical dimensions of roughly 100–200 μm on the substrates (Fig. 2c,d). The atomic flatness of the nanosheet in Fig. 2d is confirmed by a root-mean-square roughness of R_q = 0.16 nm in the atomic-force microscopy (AFM) image and height profile in Fig. 2e. Furthermore, monolayer Bi_2SeO_5 nanosheets with a thickness of roughly

https://doi.org/10.1038/s41563-023-01502-7

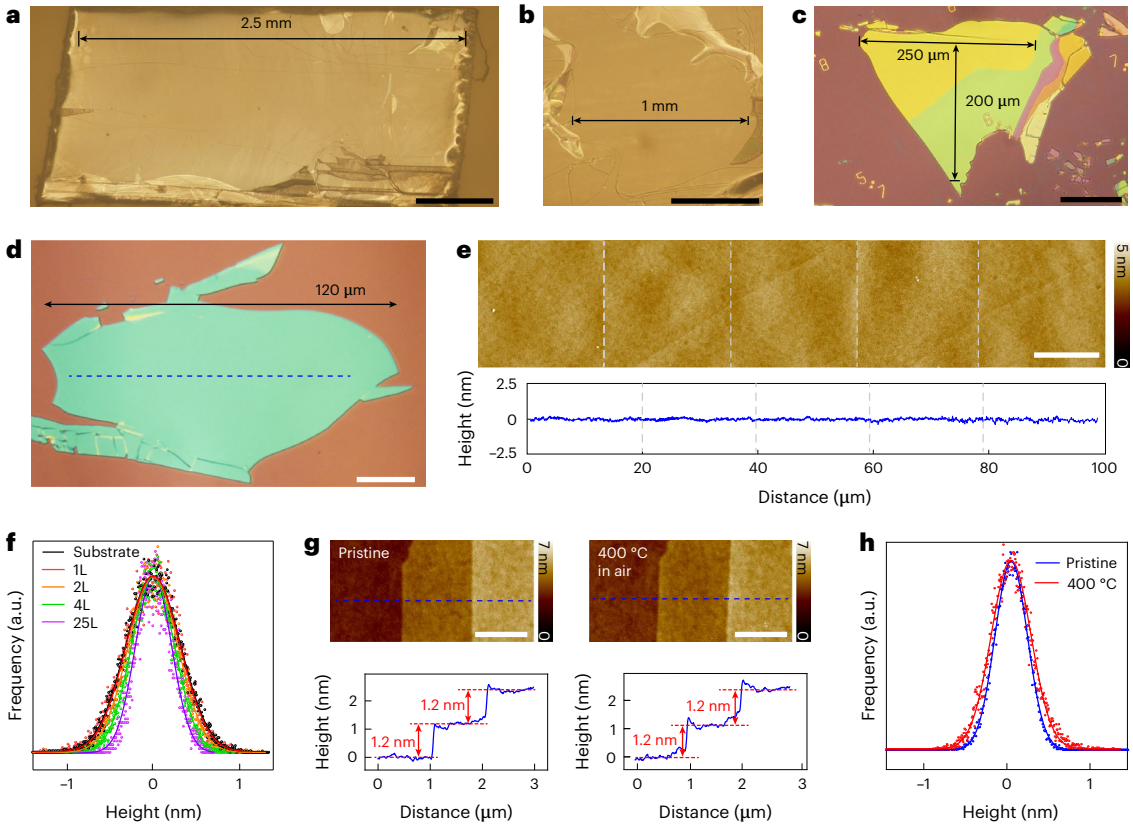

Fig. 2 | Exfoliation and characterization of vdW layered Bi_2SeO_5 nanosheets. **a**,**b**, Cleaved Bi_2SeO_5 flakes with typical scale of 2.5 mm (**a**) and 1 mm (**b**). **c**,**d**, Typical Bi_2SeO_5 nanosheets exfoliated onto Si/SiO_2 substrates with a thickness of about 180 nm (**c**) and about 30 nm (**d**). **e**, AFM image of Bi_2SeO_5 nanosheet in **d**. The image is assembled by five single-shot AFM images. A height profile of the AFM image, which corresponds to the dashed line in **d**, is shown. The image and height profile confirm the atomic flatness of Bi_2SeO_5 nanosheet in **d**. **f**, Surface roughness of the Si/SiO_2 substrate and Bi_2SeO_5 nanosheets with layer (L) numbers 1, 2, 4 and 25. Thick Bi_2SeO_5 nanosheets are better in smoothening the substrate roughness than thin ones. **g**, AFM images and height profiles along the dashed lines of Bi_2SeO_5 with monolayer-thick steps before (left) and after (right) annealing in air at 400 °C. The nearly unchanged surfaces show the thermal stability of Bi_2SeO_5 nanosheet. **h**, Surface roughness of the Bi_2SeO_5 nanosheet before (blue) and after (red) annealing, corresponding to the AFM images in **g**. Scale bars, 500 μm (**a**,**b**), 100 μm (**c**), 20 μm (**d**), 10 μm (**e**) and 1 μm (**g**).

1.5 nm (Fig. 2f and Supplementary Fig. 5) can be obtained. The atomic flatness of surface can survive harsh environments such as annealing at 400 °C in air for 10 min, exposing to air for 8 months, or immersing in water for 24 hours, showing good robustness that is crucial for practical devices (Fig. 2g,h and Supplementary Fig. 6).

The bandgap of Bi_2SeO_5 is measured to be about 3.6 eV by optical absorption spectroscopy (Supplementary Fig. 7b), which matches the theoretical estimation of a direct bandgap about 3.9 eV in ab initio calculations (Methods and Supplementary Fig. 7a). As a wide bandgap-layered oxide, the bandgap of Bi_2SeO_5 is suitable for 2D electronics given that the gate voltages are usually lower than that for bulk devices.

Using microwave impedance microscopy (MIM)[24,25], we have evaluated the effective isotropic dielectric constant κ_{eff} of the Bi_2SeO_5 nanosheets, as shown in Fig. 3a. The effective κ value decreases as the nanosheet thickness is thinner than 10 nm. This layer-dependence of κ has been observed in other layered materials[25–27] as well as traditional three-dimensional materials[28,29]. In layered materials, this observation is tentatively attributed to a suppression of cross-plane polarization in thin layered samples[25–27]. To further examine the κ value, we measure Bi_2SeO_5 samples in the form of a nanosheet, bulk single-crystal flake and polycrystal powder in classic capacitor structures as shown in Fig. 3b and Supplementary Fig. 8 (Methods). The powder shows a κ value of roughly 25.6, similar to thick nanosheets in Fig. 3a because they are both averaged along all crystal orientations. In contrast, the bulk single crystal and nanosheet (about 35 nm in thickness) show relatively lower κ values of 16.5 and 15.5, respectively. Their similarity arises from the same crystal orientations along a axis (out of plane). Note that although κ values along all directions need to be considered for a dielectric (for example, for screening Coulomb potentials of charged impurities[30,31]), the out-of-plane κ is more important for vdW dielectrics in practical electronics and the value of Bi_2SeO_5 is comparable to that of conventional gate oxide HfO_2 (κ about 16 to 25) in the silicon industry, which is much higher than that of hBN (roughly 3.5 in literature[26,32–34] and roughly 2.8 in our measurements in Fig. 3b).

Another important parameter for dielectrics is the capability to endure a large gate electric field, the maximum of which is called the breakdown field strength E_{bd}. By increasing the d.c. voltage on the capacitor (Methods and Supplementary Fig. 10), we evaluate the E_{bd} of the Bi_2SeO_5 nanosheet to a range from 10 to 30 MV cm^{-1}, which is comparable to that of dielectrics in the silicon industry such as Al_2O_3 (E_{bd} roughly 10–30 MV cm^{-1})[35] and HfO_2 (E_{bd} roughly 13 MV cm^{-1})[36]. Figure 3c summarizes a systematic comparison of vdW dielectrics in two axes of E_{bd} and κ, showing that the Bi_2SeO_5 has better dielectric parameters than hBN (refs. [26,32–34,37,38]) and the vdW molecular crystal Sb_2O_3 (ref. [39]).

The atomically flat surface, high E_{bd} and κ values suggest that 2D layered Bi_2SeO_5 qualifies as a good dielectric in 2D electronics. To this end, we have fabricated a 2D Bi_2O_2Se device with half of its channel encapsulated by Bi_2SeO_5 nanosheets (Fig. 4a). The in situ comparison shows that the Bi_2SeO_5 encapsulation notably improves Hall

https://doi.org/10.1038/s41563-023-01502-7

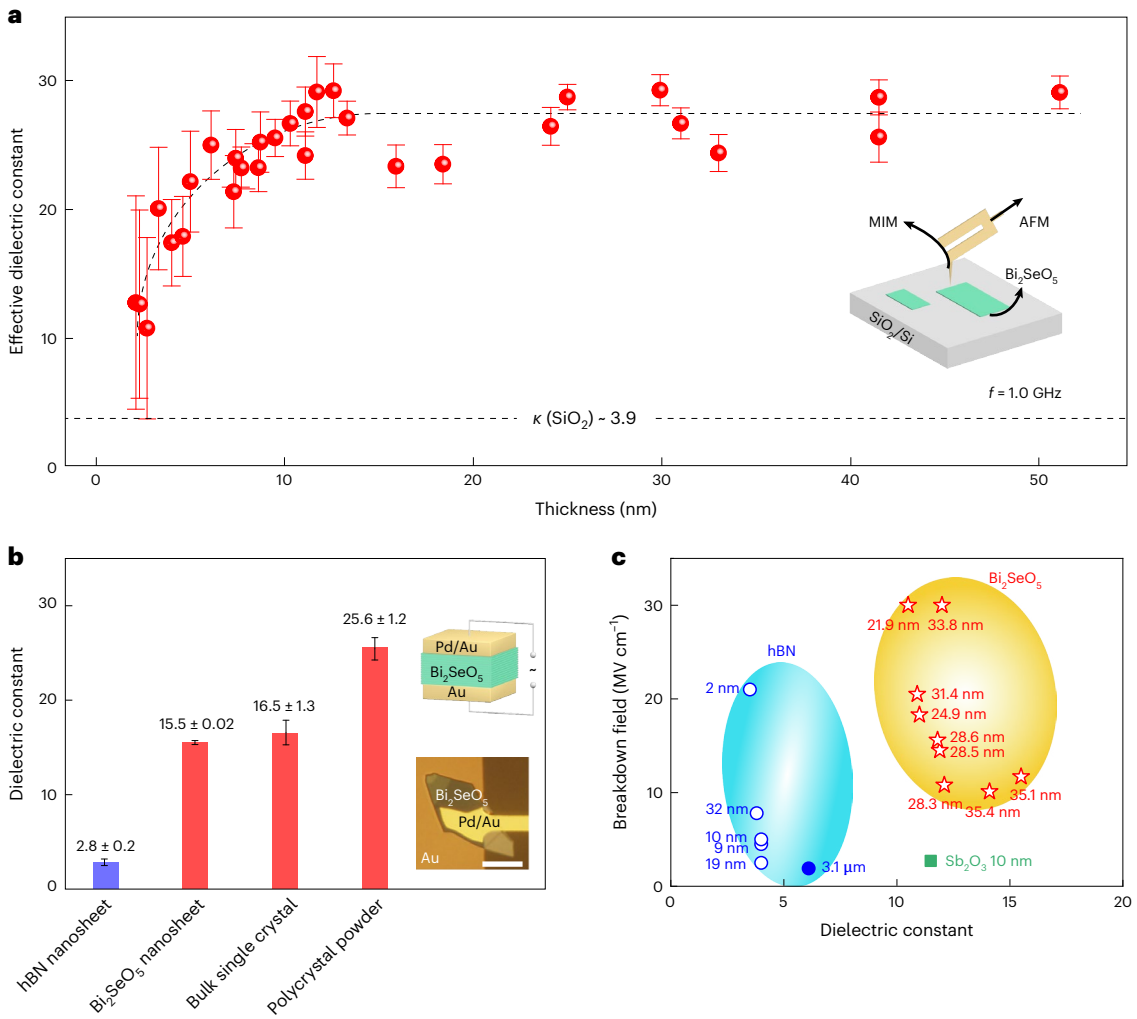

Fig. 3 | Dielectric properties of vdW layered Bi_2SeO_5. **a**, Thickness-dependent effective isotropic dielectric constant of Bi_2SeO_5 nanosheets measured by MIM. Error bars show the error of each dielectric-constant datapoint resulting from the noise of the original imaginary part of MIM signal. **b**, Dielectric constant of a hBN nanosheet, Bi_2SeO_5 nanosheet with a thickness of about 35 nm, bulk Bi_2SeO_5 single-crystal and polycrystal powder measured in a capacitor as shown by the inset diagram and optical picture. Error bars are standard deviations of κ values except the Bi_2SeO_5 nanosheet, which is the fitted error. Scale bar, 20 μm. **c**, Breakdown field strength and dielectric constant of 2D Bi_2SeO_5, 2D hBN (refs. [26,32–34,37,38]) and Sb_2O_3 (ref. [39]). All sample thickness values are labelled. No clear correlation between the thickness, the breakdown field and the dielectric constant is observed. For hBN, the out-of-plane κ values are marked with open dots, whereas averaged values involving both in-plane and out-of-plane directions are marked with solid dots.

mobility of CVD-grown 2D Bi_2O_2Se nanosheet by 250% from 43,000 to 153,000 $cm^2 V^{-1} s^{-1}$ at 1.8 K. Another CVD-grown 2D Bi_2O_2Se nanosheet device that is entirely encapsulated with Bi_2SeO_5 nanosheets shows a Hall mobility of 470,000 $cm^2 V^{-1} s^{-1}$ at 1.8 K (Fig. 4c), which is much higher than the highest mobility of 160,000 $cm^2 V^{-1} s^{-1}$ reported in ref. [40]. In addition, other 2D materials, for example, 2D MoS_2, also benefit from the encapsulation by a Bi_2SeO_5 nanosheet and show a high on/off ratio $I_{on}/I_{off} > 10^8$, low gate leakage current $<10^{-6}$ A cm^{-2}, low subthreshold swing value *SS* of roughly 70 mV dec^{-1} (Supplementary Fig. 13) and up to one order of magnitude higher mobility than a device without encapsulation (Supplementary Figs. 15–19). The improvement of 2D device performance is presumably attributed to the dangling-bond-free and atomically flat interface, as well as the high-κ dielectric environment that is more efficient in screening Coulomb scattering from charged impurities after the encapsulation with Bi_2SeO_5 nanosheets[30,41]. Moreover, the Bi_2SeO_5 dielectric with a high κ value enables a strong gate tunability. As shown in Fig. 4d, a gate voltage increase of 5.5 V (from $V_g = 4.0$ to $V_g = 9.5$ V) with a Bi_2SeO_5 dielectric thickness of about 28 nm can already induce a carrier density of 1.68×10^{13} cm^{-2} to the channel, which is several times larger than that in the device with hBN as dielectric (Supplementary Fig. 18b).

With the improved carrier mobility and high-κ environment, the advantage of the Bi_2SeO_5 vdW dielectric is directly reflected by magneto-transport results. For example, SdH quantum oscillations are much more prominent in 2D Bi_2O_2Se device when encapsulated by Bi_2SeO_5 than similar devices with hBN or SiO_2 (Fig. 4e). The QHE is observed in Bi_2O_2Se materials thanks to the high carrier mobility arising from the encapsulation of Bi_2SeO_5, as shown in Fig. 4f. The well-developed plateaus have been assigned to filling factors (ν) ranging from 42 to 70. The observation of SdH and QHE highlights the advantage of implementing 2D Bi_2SeO_5 vdW dielectric in 2D electronics.

In conclusion, single crystals of high-κ vdW layered Bi_2SeO_5 dielectrics have been synthesized with the CVT method. The single crystals have centimetre dimensions in length and low cleavage energy, facilitating the exfoliation of large dielectric layers such as those 250 × 200 μm^2 in size and monolayer in thickness. The layered dielectric shows a high dielectric constant κ of roughly 16.5, high breakdown

https://doi.org/10.1038/s41563-023-01502-7

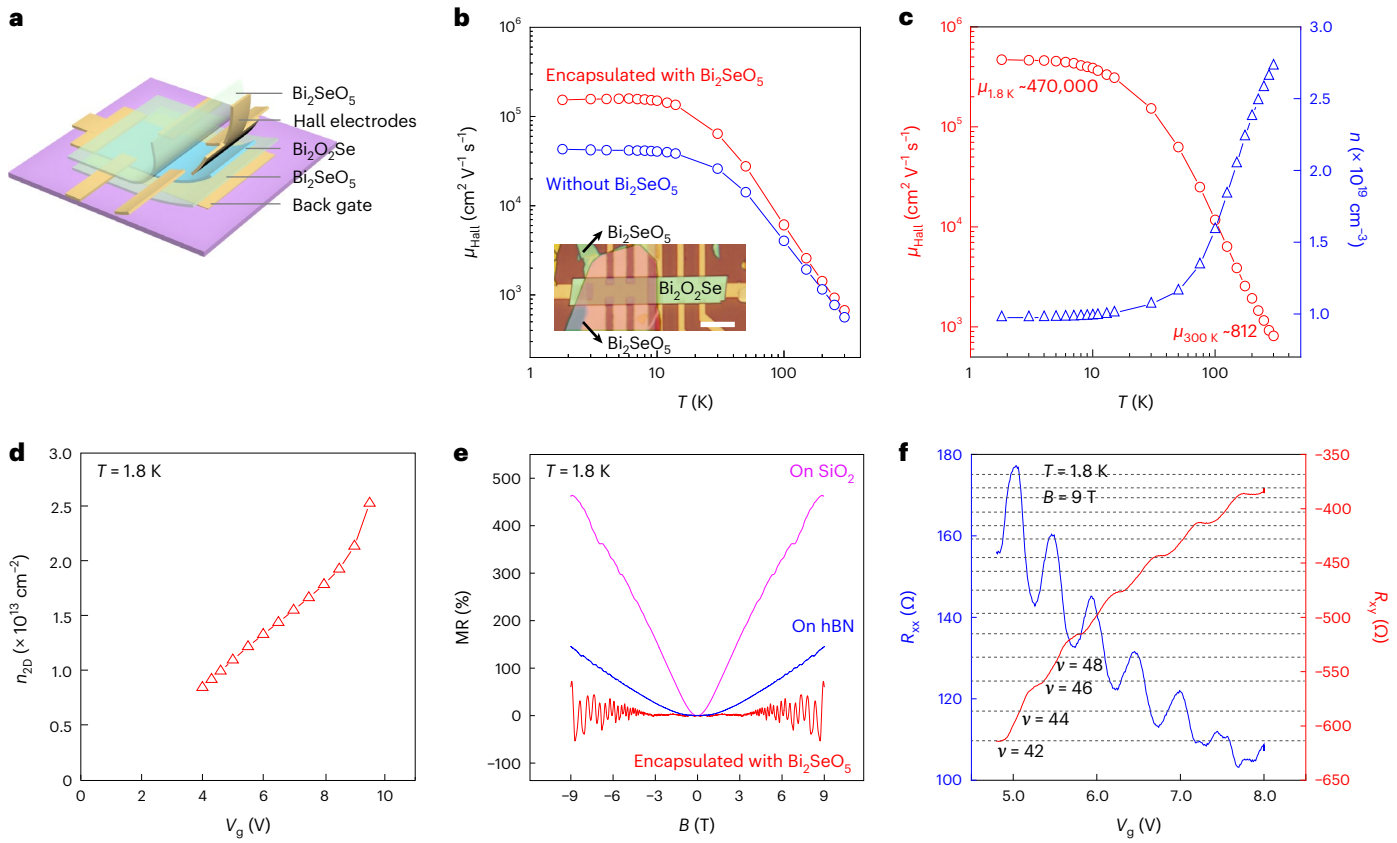

Fig. 4 | Transport properties of 2D Bi_2O_2Se encapsulated with Bi_2SeO_5 nanosheets. a, Schematic of a back-gate Bi_2O_2Se Hall bar device encapsulated with Bi_2SeO_5 nanosheets. **b**, Temperature dependent Hall mobility (μ_{Hall}) of 2D Bi_2O_2Se with and without Bi_2SeO_5 encapsulation. The inset shows an optical picture of the device. **c**, Hall mobility (μ_{Hall}) and carrier density (n) as a function of temperature in a 2D Bi_2O_2Se entirely encapsulated with a 2D Bi_2SeO_5 nanosheet. **d**, Carrier density (n_{2D}) as a function of back-gate voltage in 2D Bi_2O_2Se with a Bi_2SeO_5 nanosheet serving as the dielectric. The thickness of the dielectric is about 28 nm. **e**, Magnetoresistance (MR) in 2D Bi_2O_2Se encapsulated with Bi_2SeO_5 nanosheets (red), on hBN (blue) and on SiO_2 (purple). **f**, Hall resistance (red) and magnetoresistance (blue) as a function of V_g in 2D Bi_2O_2Se encapsulated with Bi_2SeO_5 nanosheets. The QHE with plateaus for the filling factors ν from 42 to 70 is identified.

field strength $E_{bd} > 10$ MV cm^{-1}, dangling-bond-free and atomically smooth surface, which enable an efficient control of carrier density, an increase in carrier mobility and therefore the observation of the QHE in the 2D Bi_2O_2Se materials. With these merits, 2D electronics with high carrier density, high mobility and therefore new physics are accessible. Also, the gate voltage can also be lowered in 2D electronics, which reduces the power consumption of future nanoelectronics and integrated circuits.

Online content

Any methods, additional references, Nature Portfolio reporting summaries, source data, extended data, supplementary information, acknowledgements, peer review information; details of author contributions and competing interests; and statements of data and code availability are available at https://doi.org/10.1038/s41563-023-01502-7.

References

1. Liu, Y., Duan, X., Shin, H. J., Park, S. & Duan, X. Promises and prospects of two-dimensional transistors. *Nature* **591**, 43–53 (2021).
2. Das, S. et al. Transistors based on two-dimensional materials for future integrated circuits. *Nat. Electron.* **4**, 786–799 (2021).
3. Kingon, A. I., Maria, J.-P. & Streiffer, S. K. Alternative dielectrics to silicon dioxide for memory and logic devices. *Nature* **406**, 1032–1038 (2000).
4. Illarionov, Y. Y., Knobloch, T., Jech, M., Lanza, M. & Grasser, T. Insulators for 2D nanoelectronics: the gap to bridge. *Nat. Commun.* **11**, 3385 (2020).
5. Wen, C. et al. Dielectric properties of ultrathin CaF_2 ionic crystals. *Adv. Mater.* **32**, 2002525 (2020).
6. Rhodes, D., Chae, S. H., Ribeiro-Palau, R. & Hone, J. Disorder in van der Waals heterostructures of 2D materials. *Nat. Mater.* **18**, 541–549 (2019).
7. Dean, C. R. et al. Boron nitride substrates for high-quality graphene electronics. *Nat. Nanotechnol.* **5**, 722–726 (2010).
8. Xue, J. et al. Scanning tunnelling microscopy and spectroscopy of ultra-flat graphene on hexagonal boron nitride. *Nat. Mater.* **10**, 282–285 (2011).
9. Chen, T.-A. et al. Wafer-scale single-crystal hexagonal boron nitride monolayers on Cu (111). *Nature* **579**, 219–223 (2020).
10. Lee, J. S. et al. Wafer-scale single-crystal hexagonal boron nitride film via self-collimated grain formation. *Science* **362**, 817–821 (2018).
11. Knobloch, T. et al. The performance limits of hexagonal boron nitride as an insulator for scaled CMOS devices based on two-dimensional materials. *Nat. Electron.* **4**, 98–108 (2021).
12. Wang, L. et al. One-dimensional electrical contact to a two-dimensional material. *Science* **342**, 614–617 (2013).
13. Tan, C., Adinehloo, D., Hone, J. & Perebeinos, V. Phonon-limited mobility in h-BN encapsulated AB-stacked bilayer graphene. *Phys. Rev. Lett.* **128**, 206602 (2022).

14. Li, L. et al. Quantum Hall effect in black phosphorus two-dimensional electron system. *Nat. Nanotechnol.* **11**, 593–597 (2016).
15. Bandurin, D. A. et al. High electron mobility, quantum Hall effect and anomalous optical response in atomically thin InSe. *Nat. Nanotechnol.* **12**, 223–227 (2016).
16. Benyamini, A. et al. Fragility of the dissipationless state in clean two-dimensional superconductors. *Nat. Phys.* **15**, 947–953 (2019).
17. Huang, B. et al. Electrical control of 2D magnetism in bilayer CrI_3. *Nat. Nanotechnol.* **13**, 544–548 (2018).
18. Cao, Y. et al. Unconventional superconductivity in magic-angle graphene superlattices. *Nature* **556**, 43–50 (2018).
19. Holler, B. A., Crowley, K., Berger, M. H. & Gao, X. P. A. 2D semiconductor transistors with van der Waals oxide MoO_3 as integrated high-κ gate dielectric. *Adv. Electron. Mater.* **6**, 2000635 (2020).
20. de Castro, I. A. et al. Molybdenum oxides—from fundamentals to functionality. *Adv. Mater.* **29**, 1701619 (2017).
21. Zheng, H. et al. Nanostructured tungsten oxide—properties, synthesis, and applications. *Adv. Funct. Mater.* **21**, 2175–2196 (2011).
22. Rademacher, O., Göbel, H., Ruck, M & Oppermann, H Crystal structure of dibismuth selenium pentoxide, Bi_2SeO_5. *Z. für. Kristallogr. N. Cryst. Struct.* **216**, 29–30 (2001).
23. Li, T., Tu, T., Sun, Y., Fu, H. & Peng, H. A native oxide high-κ gate dielectric for two-dimensional electronics. *Nat. Electron.* **3**, 473–478 (2020).
24. Lai, K., Ji, M. B., Leindecker, N., Kelly, M. A. & Shen, Z. X. Atomic-force-microscope-compatible near-field scanning microwave microscope with separated excitation and sensing probes. *Rev. Sci. Instrum.* **78**, 063702 (2007).
25. Wu, D. et al. Thickness-dependent dielectric constant of few-layer In_2Se_3 nano-flakes. *Nano Lett.* **15**, 8136–8140 (2015).
26. Laturia, A., Van, D. & Vandenberghe, W. G. Dielectric properties of hexagonal boron nitride and transition metal dichalcogenides: from monolayer to bulk. *NPJ 2D Mater. Appl.* **2**, 6 (2018).
27. Chen, X. et al. Probing the electron states and metal-insulator transition mechanisms in molybdenum disulphide vertical heterostructures. *Nat. Commun.* **6**, 6088 (2015).
28. Huang, J.-K. et al. High-κ perovskite membranes as insulators for two-dimensional transistors. *Nature* **605**, 262–267 (2022).
29. Stengel, M. & Spaldin, N. A. Origin of the dielectric dead layer in nanoscale capacitors. *Nature* **443**, 679–682 (2006).
30. Ma, N. & Jena, D. Charge scattering and mobility in atomically thin semiconductors. *Phys. Rev. X* **4**, 011043 (2014).
31. Yu, Z. et al. Realization of room-temperature phonon-limited carrier transport in monolayer MoS_2 by dielectric and carrier screening. *Adv. Mater.* **28**, 547–552 (2016).
32. Jang, S. K., Youn, J., Song, Y. J. & Lee, S. Synthesis and characterization of hexagonal boron nitride as a gate dielectric. *Sci. Rep.* **6**, 30449 (2016).
33. Kim, K. K. et al. Synthesis and characterization of hexagonal boron nitride film as a dielectric layer for graphene devices. *ACS Nano* **6**, 8583–8590 (2012).
34. Ahmed, F. et al. Dielectric dispersion and high field response of multilayer hexagonal boron nitride. *Adv. Funct. Mater.* **28**, 1804235 (2018).
35. Lin, H. C., Ye, P. D. & Wilk, G. D. Leakage current and breakdown electric-field studies on ultrathin atomic-layer-deposited Al_2O_3 on GaAs. *Appl. Phys. Lett.* **87**, 182904 (2005).
36. Sire, C., Blonkowski, S., Gordon, M. J. & Baron, T. Statistics of electrical breakdown field in HfO_2 and SiO_2 films from millimeter to nanometer length scales. *Appl. Phys. Lett.* **91**, 242905 (2007).
37. Ranjan, A. et al. Dielectric breakdown in single-crystal hexagonal boron nitride. *ACS Appl. Electron. Mater.* **3**, 3547–3554 (2021).
38. Worsley, R. et al. All-2D material inkjet-printed capacitors: toward fully printed integrated circuits. *ACS Nano* **13**, 54–60 (2019).
39. Liu, K. et al. A wafer-scale van der Waals dielectric made from an inorganic molecular crystal film. *Nat. Electron.* **4**, 906–913 (2021).
40. Tan, C. et al. Strain-free layered semiconductors for 2D transistors with on-state current density exceeding 1.3 mA μm^{-1}. *Nano Lett.* **22**, 3770–3776 (2022).
41. Radisavljevic, B. & Kis, A. Mobility engineering and a metal–insulator transition in monolayer MoS_2. *Nat. Mater.* **12**, 815–820 (2013).

Methods

Synthesis of Bi_2SeO_5 single crystals

Single crystals of bulk Bi_2SeO_5 were grown by the CVT method. The prereacted Bi_2SeO_5 powder was synthesized from Bi_2O_3 powder (Alfa Aesar, 99.999%) and SeO_2 powder (Alfa Aesar, 99.999%) with the molar ratio of 1:1. They were sealed in an evacuated quartz tube under vacuum and fed into a furnace (850 °C) for 12 h. For the growth of Bi_2SeO_5 single crystals, as-synthesized Bi_2SeO_5 powder was mixed with 1.5 mg cm^{-3} I_2 crystals (Energy Chemical, sublimated at 120 °C) and resealed in another evacuated quartz tube. The mixed powder was placed in the hot centre of the furnace at 860 °C for 40 d and the Bi_2SeO_5 single crystals were recrystallized at the low-temperature zone by I_2 transport.

Characterization of Bi_2SeO_5 crystals and Bi_2SeO_5 nanosheets

As-grown Bi_2SeO_5 crystals were examined by optical microscopy (Olympus DX51 microscope), field emission scanning electron microscopy (Hitachi S-4800), single-crystal X-ray diffractometer (XtaLAB PRO 007HF, Mo) and XRD (Rigaku D/Max-2000 diffractometer, Cu Kα radiation (λ = 0.15406 nm) at 40 kV and 100 mA). As-exfoliated Bi_2SeO_5 nanosheets were characterized by optical microscopy (Olympus DX51 microscope), AFM (Bruker Dimension Icon with Nanoscope V controller), spherical-aberration correction transmission electron microscopy (Titan Cubed Themis G2 300, 300 kV).

Ab initio calculations

To simulate the electronic properties of bulk Bi_2SeO_5, we first performed first-principles calculations using the Vienna ab initio simulation package in the framework of density functional theory (DFT)[42]. DFT calculations within the generalized gradient approximation were performed with the projector-augmented-wave pseudopotential. Plane waves with a kinetic energy cut-off of 400 eV were adopted as the basis set. A k-mesh grid of 3 × 10 × 5 was used for Brillouin zone sampling. The experimental lattice constants of a = 16.24 Å, b = 5.49 Å and c = 11.42 Å were adopted. Geometry optimization was carried out until the residual force on each atom was less than 0.01 eV $Å^{-1}$. To correct the underestimated bandgap by Perdew–Burke–Ernzerhof, the Heyd–Scuseria–Ernzerhof hybrid functional[43,44], HSE06, was further used, giving a direct bandgap of 3.90 eV.

The cleavage energy is defined as the energy needed to peel off a single vdW layer from the surface of a bulk material. Supplementary Fig. 3b shows the total energy as a function of interlayer distance calculated by DFT. Our calculation was based on DFT as implemented in the Vienna ab initio simulation package[45]. The Perdew–Burke–Ernzerhof type generalized gradient approximation was used for the exchange correlation energy calculation[46]. A 5 × 5 × 7 k-mesh was used for the ground state energy minimization.

Metal–insulator–metal device fabrication and electrical measurements

The metal–insulator–metal capacitors were fabricated as follows. Electron-beam lithography (EBL) was used to write Au bottom electrodes (10 nm) on the quartz substrate. Bi_2SeO_5 nanosheets were transferred onto the bottom electrodes with the help of a polypropylene carbonate/polydimethylsiloxane (PPC/PDMS) stamp and multi-axis translation stages (translation precision roughly 1 μm). The top electrodes were deposited with Pd/Au (5/50 nm) after EBL.

MIM measurements

The MIM measurements were carried out on a commercial AFM platform (Park AFM XE-70). The demodulated MIM signals were then compared to the finite-element analysis results to extract the dielectric constant at roughly 1.0 GHz. The MIM measured an effective dielectric constant κ_{eff} that is a weighted average over all directions. During the simulation, we assumed that κ_{eff} was isotropic. Since the flake thicknesses in Fig. 3a are smaller than the tip radius of roughly 100 nm, the in-plane component of κ makes a greater contribution to the MIM signals than the out-of-plane component.

Hall bar device fabrication and transport measurements

Bi_2O_2Se device. Hall electrodes (Pd/Au/Pd, 5/20/5 nm) were first deposited via EBL and e-beam evaporation on Bi_2SeO_5 nanosheet, which was exfoliated on Si/SiO_2 substrate beforehand. Then, with the help of the PPC/PDMS stamp and multi-axis translation stage, a vertically grown Bi_2O_2Se nanoplate[40] was transferred onto the Hall electrodes with a part of or the whole sample on the Bi_2SeO_5 nanosheet. Finally, another Bi_2SeO_5 nanosheet was transferred onto the Bi_2O_2Se to cap it.

MoS_2 device. The bulks of MoS_2 (SPI Company), hBN (HQgraphene Company), Bi_2SeO_5 and graphite (HQgraphene Company) were exfoliated into nanosheets on Si/SiO_2 substrates. Hall electrodes (Pd/Ag, 5/15 nm) were deposited on the hBN (or Bi_2SeO_5) nanosheet. The surfaces were cleaned by a mechanical cleaning method[47]. MoS_2 was then picked up by top hBN (or Bi_2SeO_5) and released on the top of the prefabricated electrodes. Exfoliated graphite was transferred as the top gate electrode. See the Supplementary Information for more details.

Transport measurement. A standard Lock-in method was used in a cryostat (Attocube AttoDRY 2100 system with 3DR), with the temperature ranging from 1.8 to 300 K and magnetic field up to 9 T.

Data availability

The data that support the findings of this study are available from the corresponding author upon reasonable request.

Code availability

All computational data are presented in the paper.

References

42. Kresse, G. & Hafner, J. Norm-conserving and ultrasoft pseudopotentials for first-row and transition elements. *J. Phys. Condens. Matter* **6**, 8245–8257 (1994).
43. Heyd, J., Scuseria, G. E. & Ernzerhof, M. Hybrid functionals based on a screened Coulomb potential. *J. Chem. Phys.* **118**, 8207–8215 (2003).
44. Vydrov, O. A., Heyd, J., Krukau, A. V. & Scuseria, G. E. Importance of short-range versus long-range Hartree-Fock exchange for the performance of hybrid density functionals. *J. Chem. Phys.* **125**, 074106 (2006).
45. Kresse, G. & Furthmüller, J. Efficient iterative schemes for ab initio total-energy calculations using a plane-wave basis set. *Phys. Rev. B* **54**, 11169–11186 (1996).
46. Perdew, J. P., Burke, K. & Ernzerhof, M. Generalized gradient approximation made simple. *Phys. Rev. Lett.* **77**, 3865–3868 (1996).
47. Goossens, A. M. et al. Mechanical cleaning of graphene. *Appl. Phys. Lett.* **100**, 073110 (2012).

Acknowledgements

This work was supported by the National Natural Science Foundation of China (grant nos. 21920102004, 52021006, T2188101, 52072043, 92164205, 22205011, 21733001 and 22105009), Beijing National Laboratory for Molecular Sciences (grant no. BNLMS-CXTD-202001), the Tencent Foundation (XPLORER PRIZE), National Key R&D Program of China (grant no. 2020YFA0308900), Molecular Materials and Nanofabrication Laboratory in the College of Chemistry at the Peking University, and the Electron Microscopy Laboratory of the Peking University. P.G. acknowledges support from National Key R&D Program of China (2019YFA0708200) and the National Natural Science Foundation of China (grant nos. 52125307, 11974023 and 52021006). H.F. and B.Y. acknowledge support from the National Natural Science Foundation of China (grant no. 12104072). Numerical computations

were performed on Hefei Advanced Computing Center. J. Yu and K.L. acknowledge support from the Welch Foundation grant F-1814.

Author contributions

H.P. conceived the original idea for the project. C.Z. and T.T. carried out the synthesis and structural characterization of the bulk and 2D crystals. The devices were fabricated by C.Z., J.W., Y. Zhu, Y. Zhang, X.C., X.Z. and measured by J.W. and L.C., with C.T.'s and Q.H.'s help. J. Yin and J.W. analysed the data of transport measurements. C.Z., Y. Zhu and J.Z. carried out the transfer procedure with X.W.'s and Z.L.'s help. H.F., Y.L. and B.Y. carried out the theoretical calculations. J. Yu and K.L. performed the MIM measurements. The STEM measurements were performed by M.W. and R.Z. under the direction of P.G. The manuscript was written by H.P., C.Z., J. Yin, T.T. and J.W. with input from the other authors. T.L., Q.H., H.X., H.H. and H.L. provided suggestions to the manuscript. All work was supervised by H.P. All authors contributed to the scientific planning and discussions.

Competing interests

The authors declare no competing interests.

Additional information

Supplementary information The online version contains supplementary material available at https://doi.org/10.1038/s41563-023-01502-7.

Correspondence and requests for materials should be addressed to Hailin Peng.

Peer review information *Nature Materials* thanks Takhee Lee and the other, anonymous, reviewer(s) for their contribution to the peer review of this work.